Title

Fluid and Vlasov models of low-temperature, collisionless, relativistic laser-plasma interactions

Authors

Shadwick, B.A.
Tarkenton, G.M.
Esarey, E.
et al.

Publication Date

2005-01-16

Fluid and Vlasov models of low-temperature, collisionless, relativistic laser-plasma interactions*

B. A. Shadwick,[1,2,†] G. M. Tarkenton,[1] E. Esarey,[2] and C. B. Schroeder[2]

[1]*Institute for Advanced Physics, Suite 199, 10875 US Hwy 285, Conifer, CO 80433*

[2]*Ernest Orlando Lawrence Berkeley National Laboratory*

University of California, Berkeley, CA 94720

(Dated: January 16, 2005)

Abstract

A warm fluid model suitable for describing intense laser-plasma interactions is discussed. A momentum space transformation is developed for the Vlasov–Maxwell system that leads to significant computational savings. Direct numerical solutions of the Vlasov equation are compared to the predictions of the warm fluid model and excellent agreement is found. In particular, it is found that, as predicted by the warm fluid, the bulk fields are largely insensitive to the details of the phase-space distribution. The warm fluid is compared to the particle-in-cell model and it is found that the latter model, at typical numerical resolution, predicts a momentum spread in the laser that is unphysically large.

PACS numbers: 05.20.Dd, 52.27.Ny, 52.38.-r, 52.38.Kd, 52.25.Dg

I. INTRODUCTION

The current generation of experiments (cf. Refs. 1–3) on the interaction of intense, short laser pulses with underdense plasmas access a novel physical regime where the plasma electrons experience relativistic motion while the momentum spread is quite small, and collisions are practically nonexistent. This regime stands in stark distinction to the usual setting for relativistic kinetic theories and other relativistic fluid models[4–8], where the plasma is assumed to a have relativistic thermal velocity and to be collision dominated. Such models are inappropriate for the short-pulse case since collisions rates are orders of magnitude too small to guarantee local thermodynamic equilibrium.

We have recently developed a Hamiltonian, relativistic warm fluid theory for modeling intense laser-plasma interactions.[9] This theory does not rely on a collisional closure, nor make any other thermodynamic assumptions; in particular, no equation of state is assumed. Indeed, with more than one momentum dimension, this theory describes intrinsically non-equilibrium phenomena and does not admit an equation of state. Based on the predictions of the warm-fluid model, we develop a momentum-space transformation for the Vlasov–Maxwell system, which yields significant computational savings when applied to modeling short-pulse laser-plasma interactions. Solutions of the Vlasov–Maxwell system confirm the predictions of the warm-fluid model.

II. HAMILTONIAN WARM FLUID THEORY

We begin with an overview of the warm fluid model derived by Shadwick et al.[9] The fundamental assumption in this model is that of small momentum spread. This assumption leads to a general form for phase-space distribution function

$$f(\boldsymbol{r}, \boldsymbol{p}, t) = \frac{n(\boldsymbol{r}, t)}{\sqrt{(2\pi)^3 \det \Pi}}\, g(Q), \tag{1}$$

where n is the spatial density, $Q = \delta p_i\, \delta p_j\, \Pi^{-1}_{ij}$, Π_{ij} is a non-singular positive-definite tensor, $\delta p_i = p_i - P_i$, $\boldsymbol{P}$ is the average momentum about which f has a small width, and g is some positive, integrable function. The dynamical variables in this theory are the moments

$$n(\boldsymbol{r},t) = \int d^3\boldsymbol{p}\, f(\boldsymbol{r},\boldsymbol{p},t), \tag{2a}$$

$$\boldsymbol{P}(\boldsymbol{r},t) = \frac{1}{n}\int d^3\boldsymbol{p}\, \boldsymbol{p}\, f(\boldsymbol{r},\boldsymbol{p},t), \tag{2b}$$

$$\Pi_{ij}(\boldsymbol{r},t) = \frac{1}{n}\int d^3\boldsymbol{p}\ \delta p_i\, \delta p_j\, f(\boldsymbol{r},\boldsymbol{p},t)\,. \tag{2c}$$

The assumption of small momentum spread is equivalent to assuming $|\Pi| \ll m^2c^2$. Dynamical equations for these moments are then obtained by appealing to the non-canonical Hamiltonian structure of the Vlasov–Maxwell system. The primary motivation for using this technique is the guarantee (1) of a consistent asymptotic ordering; and (2) that the moment equations will conserve energy. An additional motivation is the ease of derivation as the equations of motion are computed by taking derivatives. Somewhat remarkably, all the Vlasov–Maxwell Casimir invariants map to Casimirs of the moment system. By keeping only moments through second order, processes such as those associated with wave-particle resonance are explicitly ignored. Since the phase-velocity of the oscillations of interest is near c and a non-relativistic thermal velocity is assumed, this is not a particularly serious deficiency.

The reduction of the Vlasov–Maxwell Poisson bracket to a bracket that only involves the moments is accomplished by viewing Eq. (2) as a coordinate transformation. This allows, through the chain rule, functional derivatives with respect to f to be expressed as functional derivatives with respect to n, $\boldsymbol{P}$, and Π_{ij}. The form of f is such that the third-order moments vanish and the moment bracket is naturally closed. As a result, the reduction is exact and it follows that the moment bracket satisfies the Jacobi identity. By expanding the Hamiltonian to first order in Π_{ij}, one obtains equations of motion that are independent of the form of g. As a result, the lowest order corrections to the cold theory are universal, i.e., these corrections do not depend on the details of the distribution function. (Similar ideas have been extensively explored for the non-relativistic Vlasov–Poisson system by Jones.[10])

From the reduced bracket and the moment Hamiltonian, one obtains the equations of motion in the usual way:[9,11]

$$\begin{aligned}
\partial_t n + \nabla\cdot n\boldsymbol{u} &= 0\,, && \text{(3a)}\\
\partial_t \boldsymbol{P} + \boldsymbol{u}\cdot\nabla\boldsymbol{P} &= q\left(\boldsymbol{E} + \frac{\boldsymbol{u}}{c}\times\boldsymbol{B}\right) - \frac{1}{n}\nabla\cdot\mathsf{p}\,, && \text{(3b)}\\
\partial_t\Pi_{ij} + u_k\,\partial_k\Pi_{ij} &= -\Pi_{ik}\,\partial_j u_k - \Pi_{jk}\partial_i u_k \\
&\quad + \frac{\mathsf{p}_{ki}}{n}\,(\partial_k\mathfrak{p}_j - \partial_j\mathfrak{p}_k) + \frac{\mathsf{p}_{kj}}{n}\,(\partial_k\mathfrak{p}_i - \partial_i\mathfrak{p}_k)\,, && \text{(3c)}
\end{aligned}$$

where $\mathfrak{p}$ is the canonical momentum, $\gamma_0 = \sqrt{1 + P^2/m^2\,c^2}$,

$$u_k = \frac{P_k}{m\,\gamma_0}\left[1 - \frac{\Pi_{ii}}{2\,\gamma_0^2\,m^2\,c^2} + \frac{3}{2}\,\frac{P_i\,\Pi_{ij}\,P_j}{\gamma_0^4\,m^4\,c^4}\right] - \frac{\Pi_{ki}P_i}{\gamma_0^3\,m^3\,c^2}\,, \tag{4}$$

and the pressure tensor p is given by

$$\mathsf{p}_{ij} = \frac{n}{\gamma_0\,m}\left(\delta_{ik} - \frac{P_i\,P_k}{\gamma_0^2\,m^2\,c^2}\right)\Pi_{kj}\,. \tag{5}$$

The fields $\boldsymbol{E}$ and $\boldsymbol{B}$ are determined by Maxwell's equations from the plasma current $\boldsymbol{j} = qn\boldsymbol{u}$. As we mentioned above, these equations are independent of the details of the distribution function. We expect these equations to be valid even if the distribution is not of the form Eq. (1) provided its width is small and higher order moments are much smaller than the appropriate power of Π. We will return to this in Sect. III.

In the usual relativistic thermodynamic treatment,[4,5] the assumption of collisional dominance forces the pressure to be isotropic, and one may introduce the temperature T by $\mathsf{p}_{ij} = (nT/\gamma_0)\delta_{ij}$. Isotropy of the pressure then implies

$$\Pi_{ij} = m\,T\left(\delta_{ij} + \frac{P_iP_j}{m^2c^2}\right). \tag{6}$$

This special form for Π is not structurally stable:[9] starting from an isotropic initial condition, the evolution equations will take Π out of this form. That is, the moment equations do not correspond to local thermodynamic equilibrium as there are no collisions. The isotropy of the pressure can be interpreted as a consequence of assuming an equation of state which, in the low temperature limit, is adiabatic. It is interesting to note that in one momentum dimension, the equation of motion for Π is identical to that obtained by assuming an adiabatic equation of state. This coincidence does not persist in higher dimensions where, the pressure is intrinsically non-isotropic, it is not possible to interpret the momentum spread equations as coming from any equation of state.

A. A Quasi-static Example

To illustrate the importance of non-equilibrium effects in a low temperature plasma, we examine the response of an initially thermalized plasma to an intense short laser with frequency ω_0 and pulse with length $k_p L = 2$, such that a large wake is excited, where $\omega_p = c\, k_p$ is the plasma frequency. For simplicity, we consider the under-dense case ($\omega_p \ll \omega_0$) in one spatial dimension where the plasma response can be assumed to be quasi-static.[12] For a linearly polarized laser propagating in the z-direction, evolution equations for Π in the comoving coordinates $(t, z) \mapsto (t, \xi = t - z/c)$ can solved analytically, giving

$$\Pi_{xx} = mT_0, \tag{7a}$$

$$\Pi_{xz} = mT_0 \frac{\beta_x}{1-\beta_z} = mT_0 \frac{n}{n_0} \beta_x, \tag{7b}$$

$$\Pi_{zz} = mT_0 \frac{1+\beta_x^2}{(1-\beta_z)^2} = mT_0 \left(\frac{n}{n_0}\right)^2 (1+\beta_x^2), \tag{7c}$$

where $\boldsymbol{\beta} = \boldsymbol{P}/(mc\gamma_0)$.

Figure 1 shows (a) the density wave, and (d) the longitudinal electric field driven by a resonant Gaussian laser pulse with frequency $\omega_0 = 20\,\omega_p$ and normalized vector potential $a_0 = |q|A_0/(mc^2) = 1$ computed using the cold quasi-static model. Fig. 1(b) shows the behavior of Π for an initial temperature of 15 eV and (c) shows the corresponding pressure. The behavior of Π_{zz} is in qualitative agreement with the thermodynamics of an adiabatic process. This solution exhibits significant anisotropy in the momentum spread and little "heating." Consequently, in this regime, self-trapping of electrons in the wake (leading to dark current[13]) should not be important. Thus, provided the initial plasma temperature is sufficiently small, it should be possible to operate a laser-plasma accelerator without excessive dark current, even at large wake amplitude. Shown in Fig. 1(e) are the components Π from Eq. (6), i.e., with the assumption that the pressure is isotropic, while Fig. 1(f) shows the isotropic pressure. The clear differences between these results indicate that the assumption of local equilibrium is not justified for this case and, indeed, leads to mis-characterization of phase space. In particular, comparing Fig. 1(c) with Fig. 1(f) we see that the isotropy assumption overstates the transverse force and understates the longitudinal force. These quasi-static results have also been compared to solutions of the full time-dependent equations and good agreement was found.[14]

III. VLASOV THEORY

An important prediction of the warm fluid model is that the momentum spread does not increase substantially in the short pulse case. Moreover, since the warm fluid equations are not sensitive to the details of the distribution function, we expect this behaviour to hold for distributions that are not necessarily of the form Eq. (1). Even for rather high temperatures, the fields are quite close to those of the cold fluid.[14] This suggests that the momentum centroid of f will very nearly follow the path of the cold fluid momentum and that the spread about the centroid will remain small. Hence, it would seem advantageous to formulate the Vlasov equation in an oscillation center-like manner, but instead of just removing the fast oscillations, we should transform away *all* of the cold fluid motion. We call resulting numerical method a "moving phase-space grid."

This approach is viable in any number of dimensions, but we specialize to three phase-space dimensions (z, p_x, and p_z) and perform the transformation in two steps for clarity. The Vlasov equation for the phase-space distribution function f is

$$\frac{\partial f}{\partial t} + v_z \frac{\partial f}{\partial z} \; + \; q \left(E_x - \frac{v_z}{c} \, B_y \right) \frac{\partial f}{\partial p_x} + \; q \left(E_z + \frac{v_x}{c} \, B_y \right) \frac{\partial f}{\partial p_z} = 0 \, , \tag{8}$$

where the fields are determined from the charge density $n = \int d\boldsymbol{p}\, f$ and current density $\boldsymbol{j} = q \int d\boldsymbol{p}\, \boldsymbol{v}\, f$ through Maxwell's equations. In the first transformation we introduce $\widetilde{p}_x = p_x - \widetilde{P}_x$ and put $f(z, p_x, p_z, t) = \widetilde{F}(z, \widetilde{p}_x, p_z, t)$. For our case, the transverse cold fluid equation can be solved to give $\widetilde{P}_x = -(q/c)\, A_x$, where A_x is the vector potential, and we can write Eq. (8) as

$$\frac{\partial \widetilde{F}}{\partial t} + v_z \frac{\partial \widetilde{F}}{\partial z} + q \left(-\frac{\partial \phi}{\partial z} + \frac{p_x}{mc\,\gamma} \, \frac{\partial A_x}{\partial z} \right) \frac{\partial \widetilde{F}}{\partial p_z} = 0 \, . \tag{9}$$

Using the definition of γ, we obtain

$$\frac{\partial \widetilde{F}}{\partial t} + v_z \frac{\partial \widetilde{F}}{\partial z} - q \left(\frac{\partial \phi}{\partial z} + \frac{\partial \gamma}{\partial z} \right) \frac{\partial \widetilde{F}}{\partial p_z} = 0 \, , \tag{10}$$

where $\gamma^2 = 1 + \{p_z^2 + [\widetilde{p}_x - (q/c) A_x]^2\}/(m^2 c^2)$.

By the same means, we remove the longitudinal fluid motion. It is clearest to start with Eq. (9) rather than the more compact form Eq. (10). The equation of motion for the longitudinal momentum $\widetilde{P}_z$ can be written as

$$\frac{\partial \widetilde{P}_z}{\partial t} + \frac{\partial \left(q\, \phi + mc^2 \, \widetilde{\gamma} \right)}{\partial z} = 0 \, , \tag{11}$$

where $\widetilde{\gamma} = \sqrt{1 + \widetilde{P}^2/m^2\,c^2}$. As above, we define $\widetilde{p}_z = p_z - \widetilde{P}_z$ and put $f(z, p_x, p_z, t) = \widetilde{F}(z, \widetilde{p}_x, p_z, t) = F(z, \widetilde{p}_x, \widetilde{p}_z, t)$. The transformed Vlasov equation becomes

$$\begin{aligned} 0 \;=\; & \frac{\partial F}{\partial t} + v_z \frac{\partial F}{\partial z} \\ & + \frac{\partial F}{\partial \widetilde{p}_z} \left(mc^2 \frac{\partial \widetilde{\gamma}}{\partial z} + \frac{q\,p_x}{mc\,\gamma}\,\frac{\partial A_x}{\partial z} - \frac{p_z}{mc\,\gamma}\,\frac{\partial \widetilde{P}_z}{\partial z} \right). \end{aligned} \tag{12}$$

Under this transformation we have $\gamma^2 = 1 + \{(\widetilde{p}_z + \widetilde{P}_z)^2 + [\widetilde{p}_x - (q/c)\,A_x]^2\}/(m^2c^2)$ from which we see that the last terms in Eq. (12) can be combined to give

$$\frac{\partial F}{\partial t} + v_z \frac{\partial F}{\partial z} + \frac{\partial F}{\partial \widetilde{p}_z}\, mc^2 \frac{\partial}{\partial z}\,(\widetilde{\gamma} - \gamma) = 0\,. \tag{13}$$

It is important to understand that in this transformation, $\widetilde{P}_x$ and $\widetilde{P}_z$ are *prescribed*; it proves advantageous if they are chosen (as we have done) to solve the cold fluid equations. While it will turn out that $\widetilde{P}_x$ and $\widetilde{P}_z$ are reasonable approximations to the first moments of F; this is solely due to the nature of the problem. We have not assumed that $\widetilde{P}_x$ and $\widetilde{P}_z$ approximate the moments of F; we are simply performing an exact coordinate transformation (of course the phenomenology of the problem leads to this choice of transformation).

The attraction of this transformation as a numerical technique lies in the relative sizes of the (p_x, p_z) grid versus the $(\widetilde{p}_x, \widetilde{p}_z)$ grid. Now the $(\widetilde{p}_x, \widetilde{p}_z)$ grid will cover an area in momentum space of approximately $m\,T$, while the (p_x, p_z) grid will cover an area (due in large part to the excursion of $\widetilde{\boldsymbol{P}}$) of approximately $m^2c^2a_0^3$ in the linear case ($a_0 < 1$) and $m^2c^2a_0^2$ in the nonlinear case ($a_0 > 1$). For $T_0 = 5$ eV and $a_0 = 1.5$, the $(\widetilde{p}_x, \widetilde{p}_z)$ grid is some 10^4 times smaller. Since the resolution requirements are the same on both grids (both must resolve f), the computational savings is proportional to the ratios of the areas. For the example, this means a savings of approximately 10^4 in solving Eq. (13) over Eq. (8). It is worth reiterating that there is no approximation involved in this method and so there is no danger of inaccurate solutions being produced when the basic assumption is violated. If the momentum spread of f starts to grow significantly, then the $\widetilde{\boldsymbol{p}}$ grid will be readily seen to be too small and the appropriate steps can be taken.

As an example of this method we solve the quasi-static version of Eq. (13) and explore the extent to which the bulk fields and moment spread, as predicted by the warm fluid, are independent of the details of the distribution. We consider three initial distributions, shown in Fig. 2. In addition to the simple Maxwellian

$$f_{\text{M}} = \frac{n_0}{2\pi T} \exp\left(-\frac{\widetilde{p}^2}{2T}\right), \tag{14}$$

we take

$$\begin{aligned} f_{\text{D}} &= \frac{n_0}{2\pi T} \frac{(1+4b)}{(1+2b)^2} \exp\left(-\frac{1+4b}{1+2b}\frac{\widetilde{p}_x^2+\widetilde{p}_z^2}{2T}\right) \\ &\times \left[1+\frac{b\,(1+4b)}{1+2b}\frac{\widetilde{p}_x^2+\widetilde{p}_z^2}{T}\right] \end{aligned} \tag{15}$$

and

$$\begin{aligned} f_{\text{TS}} &= \frac{n_0}{2\pi\,(a+b)\sqrt{T\,(T-a\,b\,p_0^2)}} \times \\ &\left\{ b\,\exp\left[-\frac{{p_z}^2}{2T} - \frac{(p_x+a\,p_0)^2}{2\,(T-a\,b\,p_0^2)}\right] \right. \\ &\left. + a\,\exp\left[-\frac{{p_z}^2}{2T} - \frac{(p_x-b\,p_0)^2}{2\,(T-a\,b\,p_0^2)}\right]\right\} \end{aligned} \tag{16}$$

as initial conditions, where a, b, p_0, and T are constants. Like the Maxwellian, these latter distributions have $\Pi_{xx} = \Pi_{zz} = m\,T$ and $\Pi_{xz} = 0$. While f_{D} is of the form Eq. (1), clearly f_{TS} is not.

Shown in Fig. 3 are representative sections of phase space for the Maxwellian initial condition. The plasma wave is clearly evident in both sections, while the quiver motion, and the accompanying fine scale structure in f, is clearly visible in Fig. 3(b). Fig. 4 shows the density (a) and average longitudinal momentum (b) for all three initial conditions. Fig. 5 shows the longitudinal momentum spread for the three initial conditions. There is essentially no difference in both the bulk fields and momentum spread for these very different distributions. Fig. 6 shows the density (a) and longitudinal momentum (b) for a Maxwellian initial condition for temperatures of 5 eV, 50 eV, and 500 eV. Again we see virtually no difference in the bulk behaviour. Not only are the bulk fields insensitive to the details of the distribution, they are largely insensitive to the width as well. This behaviour results from the relatives sizes of the pressure and Lorentz forces. For an intense laser, the Lorentz force dwarfs the the pressure force at all but the highest temperatures.[14] This result has serious implications for the benchmarking of kinetic models for use in low temperature laser-plasma interactions. To be effective, benchmarks must look beyond the bulk fields and be carefully chosen to ensure sensitivity to the distribution function. This is essential as many processes of interest, such as all optical injectors, self trapping phenomena, etc., depend on the details of phase-space and are commonly modeled numerically.

IV. BENCHMARKING PIC

Now that we have solutions of the Vlasov equation in a parameter regime of direct relevance to high intensity, short-pulse laser-plasma interactions, it is logical to compare these solutions to the predictions of other kinetic models. Because of its widespread use, the particle-in-cell (PIC) model is the natural candidate for this comparison. In the following examples we use a one dimensional version of the OOPIC code.[15,16] Due to space limitation we present an overview of the results of our comparison; the details will be published elsewhere.[17] We consider a resonant ($k_p\, L = 2$) Gaussian laser pulse in under-dense regime with $a_0 = 1$, $\omega_0 = 10\,\omega_p$, and initial temperature of 10 eV. Reconstructing the phase-space distribution from a PIC model would require an impractically large number of particles, so instead we consider the second moments of the distribution which, in this case, are well described by quasi-static expressions.[9] To meaningfully compare the momentum spread to the analytical result, we must coarse-grain the particle distribution in space. We take care to choose the spatial bin size to be small enough that the binning artifacts (which are manifest as contributions to the momentum spread) are smaller than the intrinsic momentum spread.

The numerical parameters for the cases shown are summarized in Table I. Shown in Fig. 7 are the hydrodynamic quantities for both the lowest and highest resolutions at cases $\omega_p\, t = 19\pi/2$. Aside from a slight phase shift (due to the dependence of the numerical group velocity on Δz), we see that the hydrodynamic quantities are reasonably accurate even at low resolution. Notice there is more noise (most easily seen in the density but also visible in the momentum) in the high-resolution case even though N_p is the same in both cases. Fig. 8 shows the longitudinal momentum spread for the resolutions of Table I superimposed on the quasi-static prediction. The quasi-static response is computed using the average momentum from each simulation. We see that at the lower resolutions, the momentum spread inside the laser pulse is significantly too large. This error appears to scale quadratically with Δz, which indicates the source is related to truncation error in the PIC algorithm. The ratio of Δz to Δt is fixed at $c/2$. Thus, from these results alone we can not isolate the source of the error. Preliminary results (not shown) suggest this error scales quadratically with Δt, which leads us to believe that the origin the is particle advance. We are pursuing this matter further and will report our findings in a future publication.[17] Behind the laser, the momentum spread is quite close to the quasi-static result (which rules out grid heating as the source) even in the low resolution case. This error in the momentum spread has the qualitative effect of raising the plasma temperature and thus can lead to spurious trapping at higher amplitudes.

V. CONCLUSIONS

We have reviewed a recently developed a warm fluid model that treats the momentum spread of the distribution asymptotically. This model does not rely on a collisional closure and can describe non-equilibrium phenomena. In this model the distribution function and pressure are intrinsically anisotropic. The model predicts that the plasma response is largely insensitive to the details of the phase-space distribution. In addition, it predicts little heating in response to a short laser pulse. We have developed a new formulation for the Vlasov–Maxwell equations (the *moving phase-space grid*), where the bulk motion in momentum space is removed by an exact transformation. Numerical methods based on this formulation are orders of magnitude less computationally demanding than those that solve the Vlasov equation on a fixed phase-space grid. Using this method we have solved the Vlasov–Maxwell equations for various initial distributions and confirmed the prediction of the warm fluid model that the bulk fields are insensitive to the details of the distribution. In the quasi-static case, we have shown excellent agreement between the solution of the warm fluid equations and those of the Vlasov equation.

We have begun a preliminary comparison between Vlasov–Maxwell and the PIC model. Our results show that truncation errors in the particle advance result in excessively large momentum spread within the laser. At high laser intensity, this can lead to spurious trapping. Mitigation of the momentum spread error may require unacceptably high resolution in a second order PIC code suggesting the need to develop higher-order methods for PIC models.

Acknowledgments

The authors gratefully acknowledge discussions with P. J. Morrison, W. P. Leemans, E. Michel, R. D. Hazeltine, and W. B. Mori. We would also like to thank Raoul Trines for kindly providing the OOPIC code and for related discussions. This work was supported by the Institute for Advanced Physics and by the U. S. DoE under contract No. DE-AC03-76SF0098.

---

* Paper FI1B 2, Bull. Am. Phys. Soc. **49**, 135 (2004).

† Electronic address: `BAShadwick@IAPhysics.org`; Invited speaker.

[1] S. P. D. Mangles, C. D. Murphy, Z. Najmudin, A. G. R. Thomas, J. L. Collier, A. E. Dangor, E. J. Divall, P. S. Foster, J. G. Gallacher, C. J. Hooker, et al., Nature **431**, 535 (2004).

[2] C. G. R. Geddes, Cs. Toth, J. van Tilborg, E. Esarey, C. B. Schroeder, D. Bruhwiler, C. Nieter, J. Cary, and W. P. Leemans, Nature **431**, 538 (2004).

[3] J. Faure, Y. Glinec, A. Pukhov, S. Kiselev, S. Gordienko, E. Lefebvre, J.-P. Rousseau, F. Burgy, and V. Malka, Nature **431**, 541 (2004).

[4] S. R. de Groot, W. A. van Leeuwen, and Ch. G. van Weert, *Relativistic Kinetic Theory: Principles and Applications* (North-Holland, New York, 1980), ISBN 0-444-85453-3.

[5] D. Mihalas and B. Weibel-Mihalas, *Foundations of Radiation Hydrodynamics* (Dover, Mineola, New York, 1984).

[6] S. M. Mahajan, Phys. Rev. Lett. **90**, 035001 (2003).

[7] R. D. Hazeltine and S. M. Mahajan, Astrophys. J. **567**, 1262 (2002).

[8] S. M. Mahajan and R. D. Hazeltine, Phys. Plasmas **9**, 1882 (2002).

[9] B. A. Shadwick, G. M. Tarkenton, and E. H. Esarey, Phys. Rev. Lett. **93**, 175002 (2004), URL `http://link.aps.org/abstract/PRL/v93/e175002`.

[10] C. S. Jones, Ph.D. thesis, Univeristy of Texas, Austin (2003), URL `http://www.lib.utexas.edu/etd/d/2003/jonescs036/jonescs036.pdf`.

[11] B. A. Shadwick, G. M. Tarkenton, and E. Esarey, *Reduced Hamiltonian models of low-temperature relativistic plasmas*, in preparation.

[12] E. Esarey, P. Sprangle, J. Krall, and A. Ting, IEEE Trans. Plasma Sci. **24**, 252 (1996).

[13] C. B. Schroeder, E. Esarey, B. A. Shadwick, and W. P. Leemans, *Trapping and dark current in nonlinear plasma waves*, in *Advanced Accelerator Concepts, Tenth Workshop* (Aip, Melville, NY, 2004), AIP Conference Proceedings, in press.

[14] B. A. Shadwick, G. M. Tarkenton, and E. H. Esarey, *Thermal effects in intense laser-plasma interactions*, in *Advanced Accelerator Concepts, Tenth Workshop* (AIP, Melville, NY, 2004), AIP Conference Proceedings, in press.

[15] J. P. Verboncoeur, A. B. Langdon, and N. T. Gladd, Comput. Phys. Commun. **87**, 199 (1995).

[16] R. M. G. M. Trine (2004), private communication.

[17] B. A. Shadwick *et al.*, *Effects of truncation error in particle orbit integration in low temperature plasmas*, in preparation.

Figures

FIG. 1: Quasi-static plasma response to a resonant ($k_p L = 2$) Gaussian laser pulse with frequency $\omega_0 = 20\,\omega_p$ and dimensionless vector potential $a_0 = 1$: (a) density, n/n_0; (b) Π_{ij}/m from Eq. (7); (c) p_{ij}/n_0 corresponding to Π in (b); (d) longitudinal electric field, E_z/E_0 ($E_0 = c\,m\,\omega_p/q$ is the cold wavebreaking field); (e) Π_{ij}/m from Eq. (6), assuming an isotropic pressure; and (f) pressure assuming isotropy, p/n_0. (See Ref. 14.)

FIG. 2: Various initial distribution all with $T = 50$ eV: (a) $f_{\rm M}$; (b) $f_{\rm D}$ with $b = 2$; and (c) $f_{\rm TS}$ with $a = 0.5$, $b = 1.5$ and $p_0 = 0.01 m\,c$.

FIG. 3: The phase distribution function (a) at $\widetilde{p}_x = 0$ and (b) at $\widetilde{p}_x = 0.02$ obtained from solving Eq. (12) for a resonant laser pulse with $a_0 = 1$ and $\omega_0 = 10\,\omega_p$. The initial distribution was $f_{\rm M}$ with $T = 50$ eV [see Fig. 2(a)]. The fine scale phase-space structure of the distribution function due to the quiver motion is clearly visible.

FIG. 4: The density, n/n_0, (a) and longitudinal momentum, P_z/mc, (b) for the initial distributions shown in Fig 2: $f_{\rm M}$ (solid red); $f_{\rm D}$ (dashed green); and $f_{\rm TS}$ (dashed blue).

FIG. 5: Longitudinal momentum spread, Π_{zz}/m, for the initial distributions shown in Fig 2: $f_{\rm M}$ (solid red); $f_{\rm D}$ (dashed green); and $f_{\rm TS}$ (dashed blue).

FIG. 6: The density, n/n_0, (a) and longitudinal momentum, P_z/mc, (b) for Maxwellian initial distributions with temperatures of 5 eV (solid red), 50 eV (dashed green), and 500 eV (dashed blue). The bulk fields exhibit little sensitivity to temperature.

FIG. 7: Hydrodynamic quantities from PIC simulations: (a) $P_z/m\,c$, and (b) n/n_0 for $\Delta z = \lambda_0/20$, $N_p = 400$; (c) $P_z/m\,c$, and (d) n_e/n_0 for $\Delta z = \lambda_0/160$, $N_p = 400$. All quantities are shown at $\omega_p\,t = 19\pi/2$.

FIG. 8: Longitudinal momentum spread from PIC simulations shown in Fig. 7 (red) and corresponding quasi-static results (blue) for various resolutions: (a) $\Delta z = \lambda_0/20$, $N_p = 400$; (b) $\Delta z = \lambda_0/40$, $N_p = 800$; (c) $\Delta z = \lambda_0/80$, $N_p = 400$; and (d) $\Delta z = \lambda_0/160$, $N_p = 400$.

Tables

TABLE I: Grid resolutions Δz, and number of particles-per-cell N_p, for the results shown in Figs. 7 and 8. In all cases, $c\,\Delta t = \frac{1}{2}\,\Delta z$.

$\lambda_0/\Delta z$	N_p
20	400
40	800
80	400
160	400

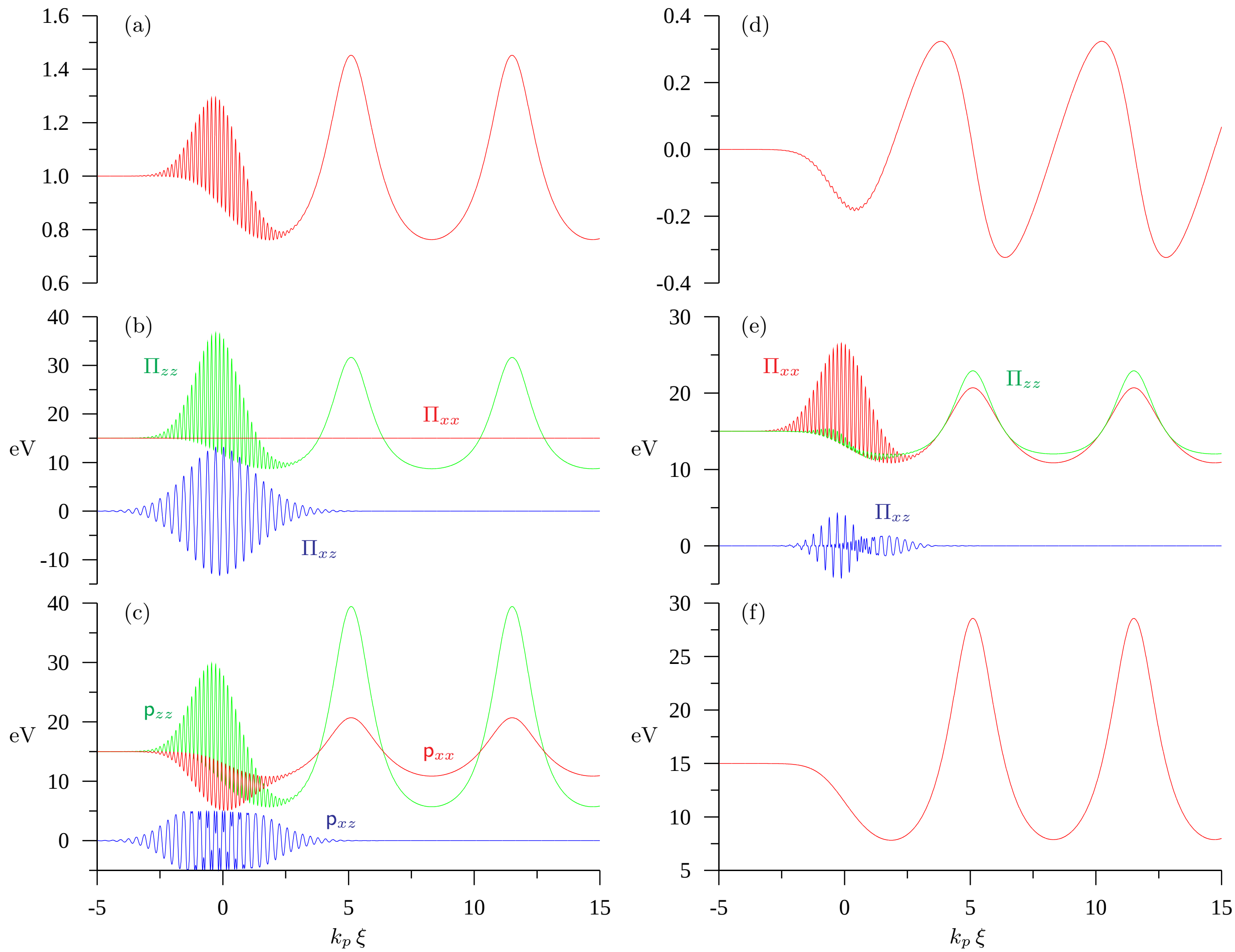
(a)
(b)
(c)
(d)
(e)
(f)
Π_{zz}
Π_{xx}
Π_{xz}
p_{zz}
p_{xx}
p_{xz}
eV
$k_p\,\xi$

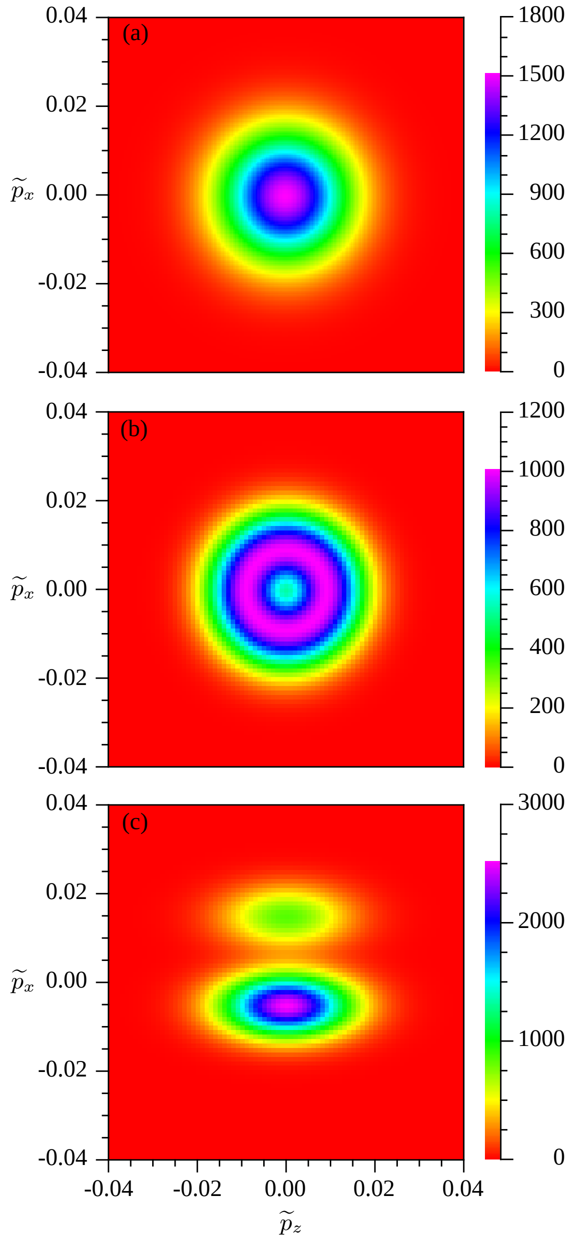
(a)
(b)
(c)
0.04
0.02
0.00
-0.02
-0.04
$\widetilde{p}_x$
$\widetilde{p}_z$
1800
1500
1200
900
600
300
0
1000
800
400
200
3000
2000

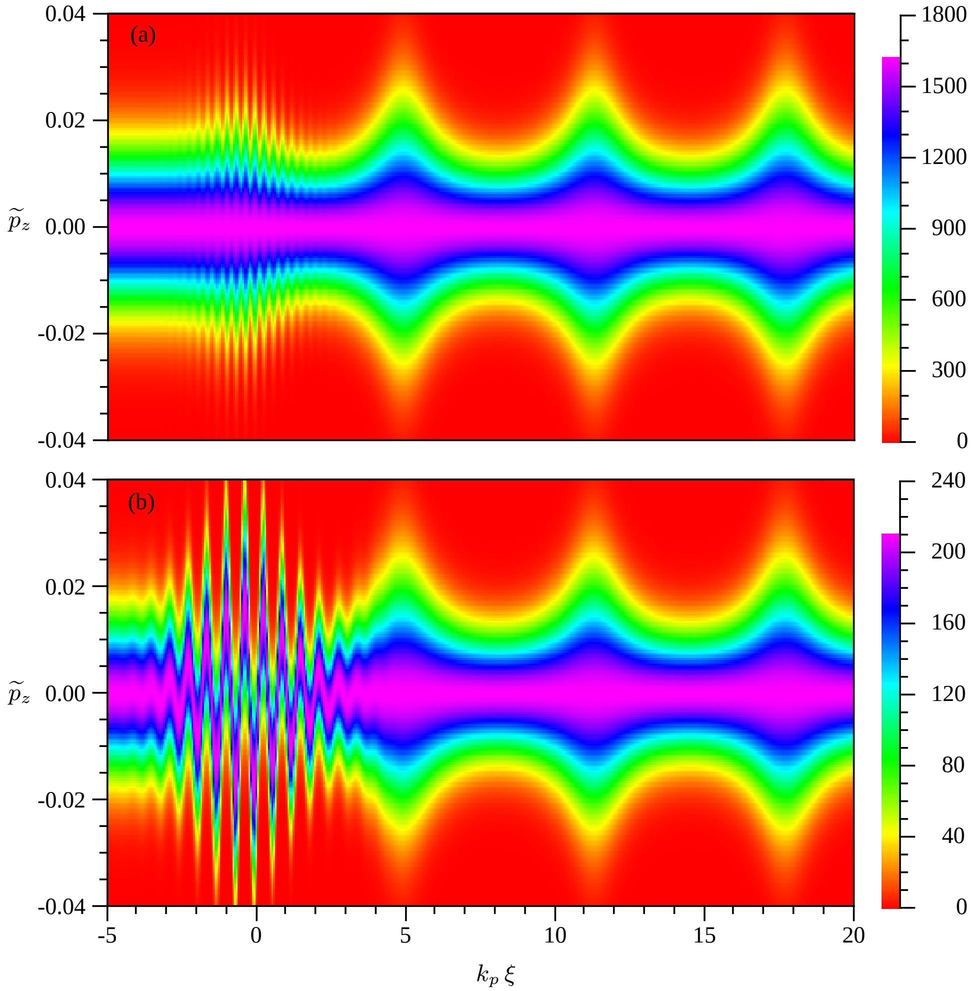

(a)
(b)
0.04
0.02
0.00
-0.02
-0.04
$\widetilde{p}_z$
1800
1500
1200
900
600
300
0
240
200
160
120
80
40
-5
5
10
15
20
$k_p\,\xi$

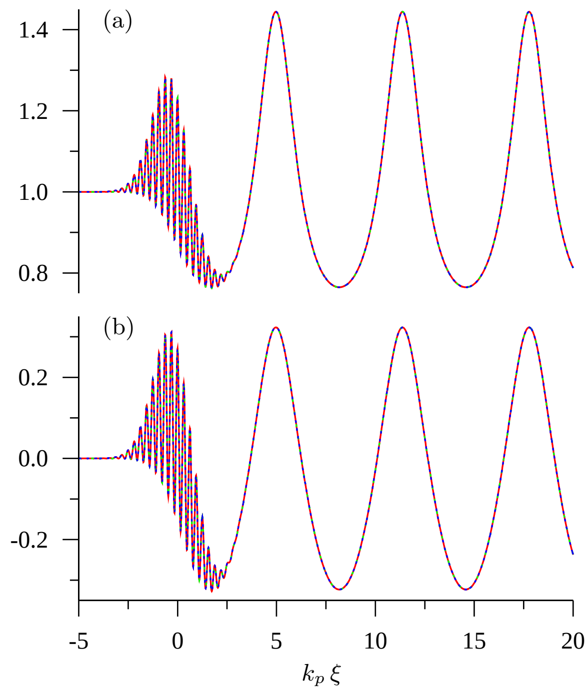

(a)
1.4
1.2
1.0
0.8
(b)
0.2
0.0
-0.2
-5
0
5
10
15
20
$k_p\,\xi$

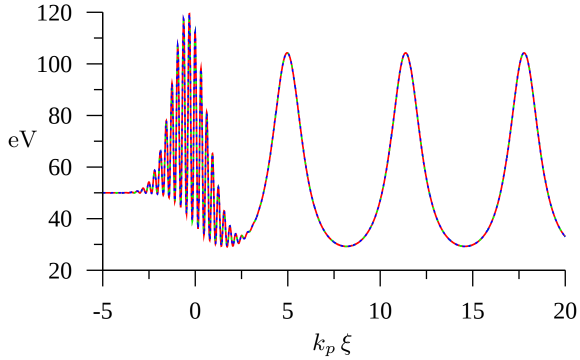
120
100
80
60
40
20
eV
-5
0
5
10
15
20
$k_p\,\xi$

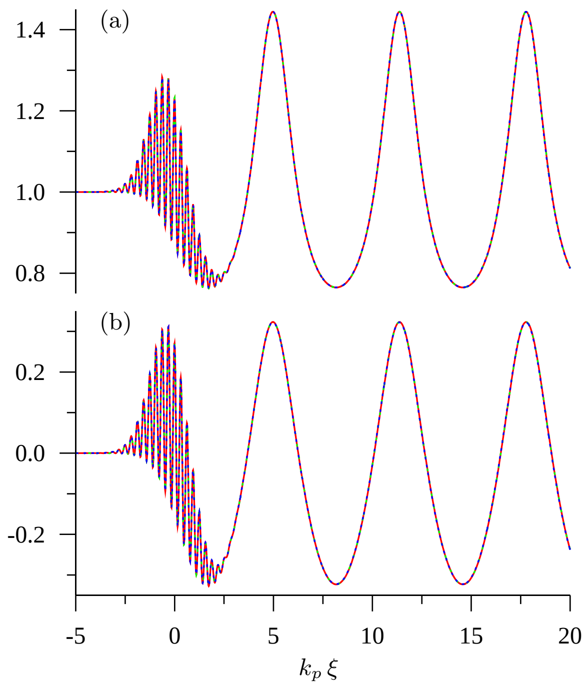

(a)
1.4
1.2
1.0
0.8
(b)
0.2
0.0
-0.2
-5
0
5
10
15
20
$k_p\,\xi$

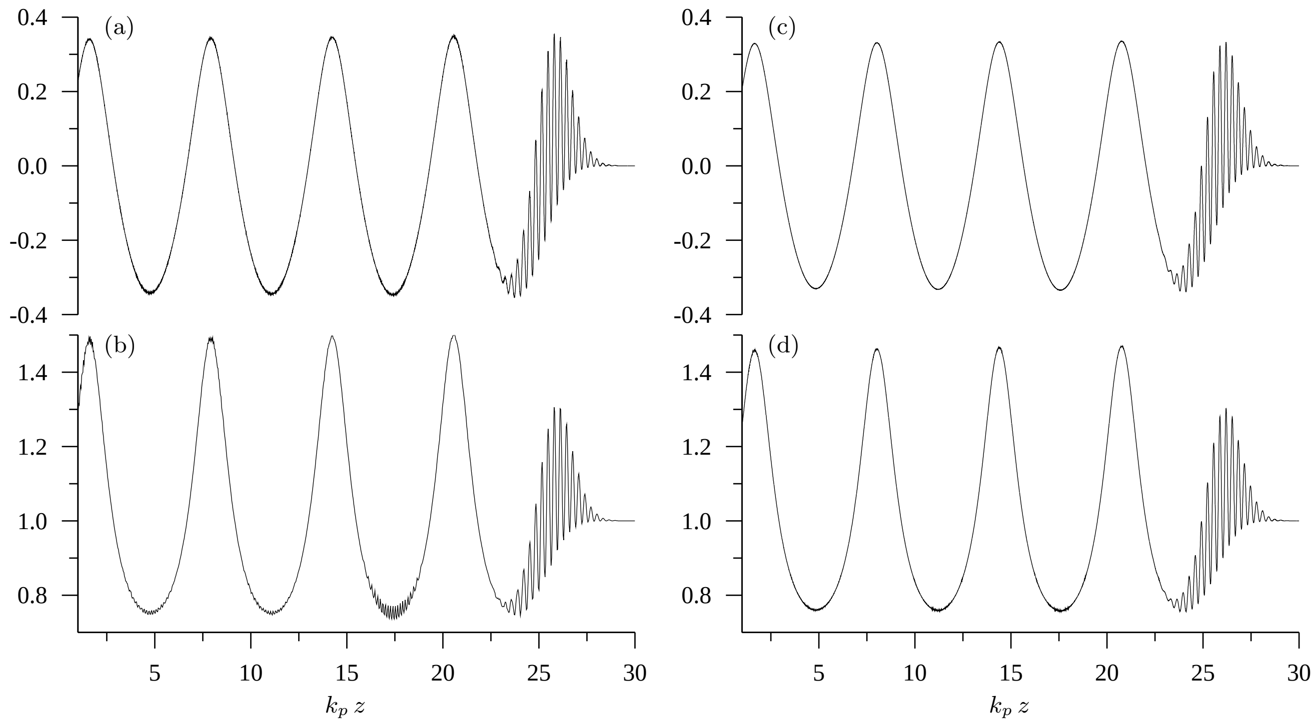
(a)
(b)
(c)
(d)
0.4
0.2
0.0
-0.2
-0.4
1.4
1.2
1.0
0.8
5
10
15
20
25
30
$k_p\, z$

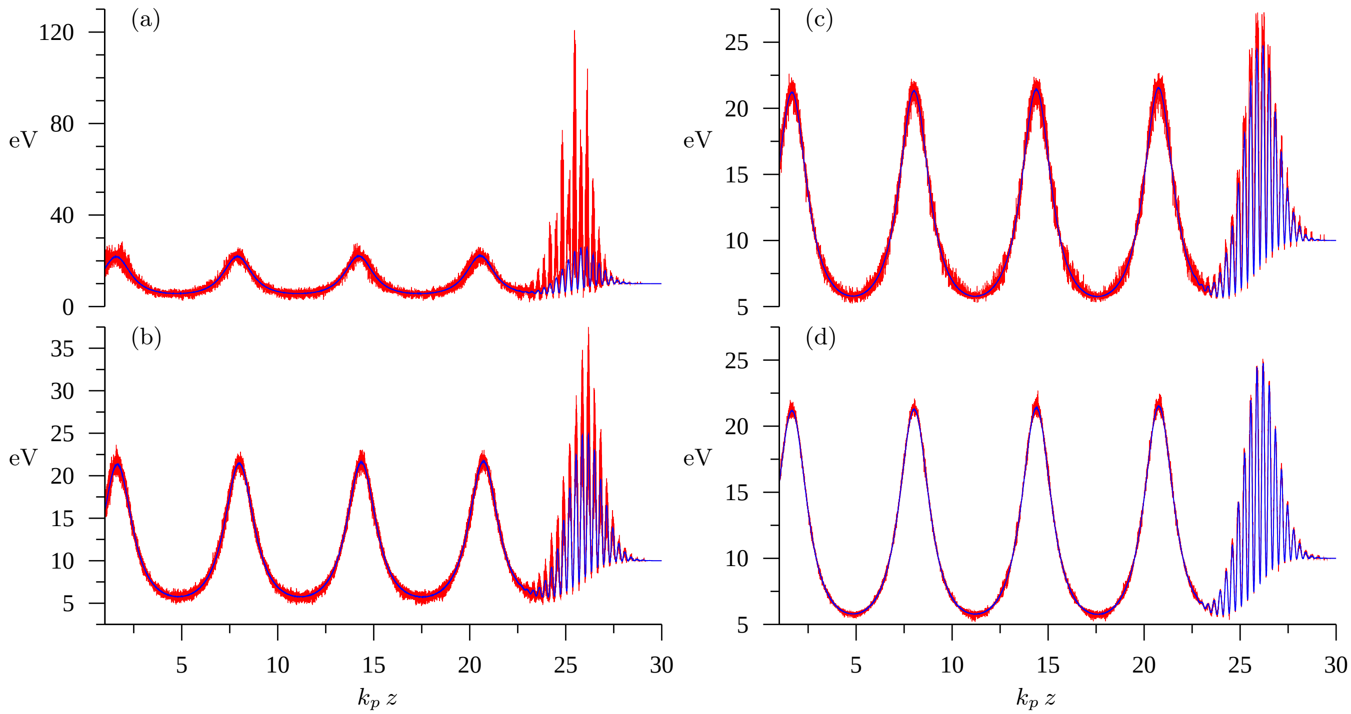

(a)
(b)
(c)
(d)
eV
$k_p\,z$